Fully Reconfigurable Waveguide Bragg Gratings for Programmable Photonic Signal Processing

Jianping Yao, *Fellow, IEEE, Fellow, OSA*, and Weifeng Zhang, *Member, IEEE*

(Invited Paper)

***Abstract*—Fiber Bragg gratings have been invented for over three decades now and have been intensively employed in optical communication and sensor systems. The key limitation of a fiber Bragg grating is that once fabricated, it is hard to be tuned or with very limited tunability via thermal or mechanical tuning. Recently, great efforts have been directed into the study of realizing Bragg gratings on silicon-on-insulator (SOI) platform. The key advantage of Bragg gratings based on SOI is that the gratings can be fast and electrically reconfigured with the use of free-carrier plasma dispersion effect in silicon, which can be employed for fast programmable photonic signal processing. In this article, Bragg gratings based on SOI that are electrically programmable will be reviewed and their use for advanced programmable optical and microwave signal processing will be discussed.**

***Index Terms*—Bragg gratings, microwave photonics, optical signal processing, photonic integrated circuits, silicon photonics.**

I. Introduction

FIBER Bragg gratings since the invention over 30 years ago [1] by Hill *et al.* have been extensively employed for various applications such as optical filtering [2]–[4], dispersion compensation [5], [6], distributed fiber-optic sensing [7]–[10], and microwave photonic signal processing [11]–[14]. Among the numerous functions that a Bragg grating can provide, signal processing is one of the most important functions, which is realized by using the spectral response of a Bragg grating to introduce a frequency-dependent loss, a frequency-dependent time delay or phase shift to an optical or microwave signal to be processed. The major limitation of using a fiber Bragg grating to perform signal processing is its limited reconfigurability. Once fabricated, the spectral response can be hardly tuned or with limited tunability via temperature or mechanical tuning.

From the beginning of this century, with the rapid development of semiconductor technologies, especially significant advancement in silicon photonics, Bragg gratings have been brought to the on-chip integration era based on silicon photonics [15], [16]. Different integrated Bragg gratings have been reported and implemented on silicon-on-insulator (SOI) platform [17]–[25]. The key advantage of implementing a Bragg grating on silicon is that the grating can be electrically reconfigured, which can be employed for programmable photonic signal processing. In this paper, recent advances in integrated Bragg gratings based on silicon photonics will be reviewed including two fully reconfigurable waveguide gratings implemented on SOI platforms and their use for advanced programmable signal processing [26], [27].

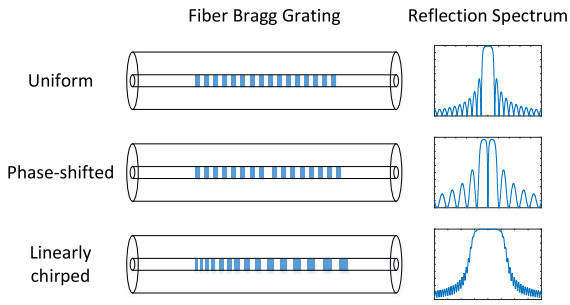

Fig. 1. Schematic diagram to show the structures and the reflection spectra of a uniform, a phase-shifted, and a chirped FBG.

II. Fiber Bragg Gratings

A fiber Bragg grating (FBG) is a fiber-optic device that is fabricated by modulating the refractive index of a fiber core via UV illumination [28]. Perturbation of refractive index inspires mode coupling between two counter-propagation modes in a fiber core. According to different mode coupling conditions, FBGs can be generally classified into two groups: 1) uniform and phase-shifted FBGs, which support strong mode coupling within very narrow bandwidth due to the uniform grating period, and 2) chirped FBGs, where broadband mode coupling is enabled due to the varying grating period. A schematic diagram to show the structures and reflection spectra of a uniform, a phase-shifted and a chirped FBG is given in Fig. 1.

FBGs have been extensively investigated since their discovery in 1978 [1]. Thanks to the important and unique features including flexible spectral characteristics [29], all-fiber geometry, low insertion loss, compact size, and low cost, FBGs have widely

Manuscript received August 3, 2019; revised December 4, 2019; accepted December 16, 2019. Date of publication December 19, 2019; date of current version January 23, 2020. This work was supported by the Natural Sciences and Engineering Research Council of Canada (NSERC). *(Corresponding author: Jianping Yao.)*

The authors are with Microwave Photonics Research Laboratory, School of Electrical Engineering and Computer Science, University of Ottawa, Ottawa, ON K1N 6N5, Canada (e-mail: jpyao@uottawa.ca; weifeng.zhang@bit.edu.cn).

Color versions of one or more of the figures in this article are available online at http://ieeexplore.ieee.org.

Digital Object Identifier 10.1109/JLT.2019.2960933

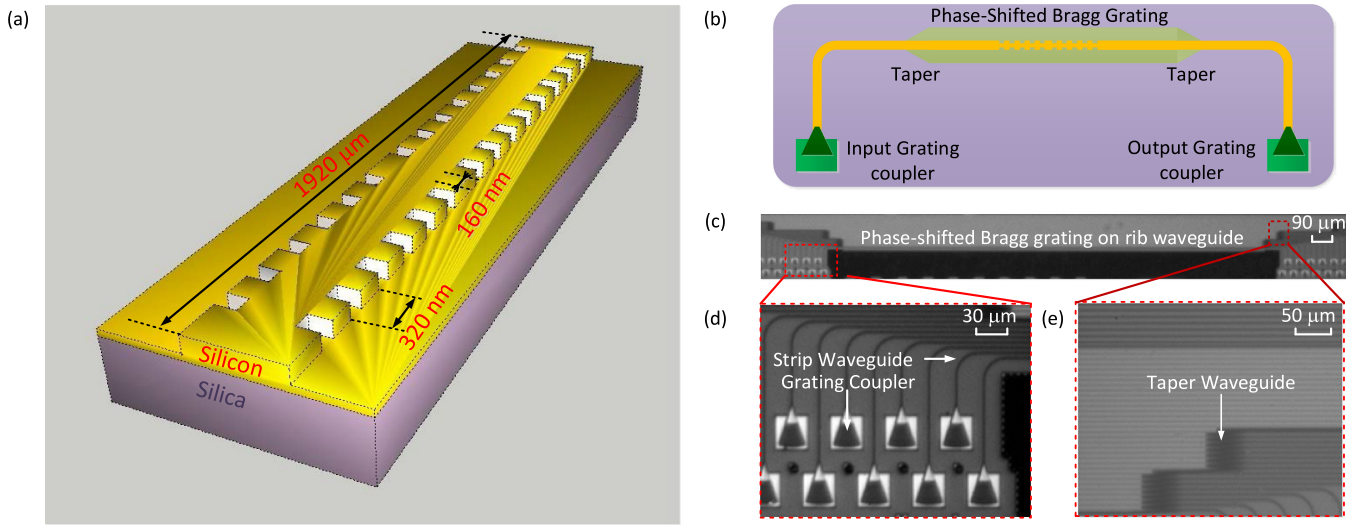

Fig. 2. (a) Perspective view of a PS-WBG in a SOI rib waveguide. (b) Schematic layout of the designed PS-WBG. (c) Image of the fabricated PS-WBG. (d) Zoom-in view of the grating couplers and the strip waveguides. (e) Zoom-in view of taper waveguides. [33].

been used, such as in fiber-optic communications systems [30], optical sensors [31], and photonic signal processors [32]. However, since FBGs are fiber optic devices, systems using FBGs are not fully integrated. In addition, a FBG, once fabricated, can be hardly tuned. For many applications, it is highly desirable that the systems are fully integrated using photonic integrated circuits (PICs). Bragg gratings in the systems, which should also be electronically tunable or reconfigurable. A solution is to implement Bragg gratings on PICs.

III. Waveguide Bragg Gratings

Thanks to the compatibility with the current CMOS technology and its potential of seamless integration with electronics, silicon photonics offers a universal photonic integration platform that enables integration of photonic modules and systems. One important device in a photonic module or system is Bragg gratings. In particular, due to the large refractive index contrast between silicon (n∼3.47) and silica (n∼1.45), a silicon-based waveguide Bragg grating usually has a strong index modulation for broadband operation with a small footprint, which is of key benefit to large-scale and high-density integration on a chip.

A silicon-based phase-shifted waveguide Bragg grating (PS-WBG) was recently demonstrated [33]. The perspective view of the device is shown Fig. 2(a). As can be seen the grating is realized by introducing periodic sidewall corrugations to a rib waveguide, which is different from an FBG in which the grating is produce by changing periodically the refractive index. A phase-shifted block, with a length corresponding to half of the grating period, is allocated at the center of the grating, to introduce a π phase shift. Fig. 2(b) shows the layout of the PS-WBG. At the two ends of the grating, there are two grating couplers to couple optical signals into and out of the chip. To minimize the chip footprint and to reduce the bending loss, a strip waveguide is mostly used to guide an optical signal from the input grating coupler to the grating and from the grating to the output grating coupler. Since the PS-WBG is realized in the rib waveguide, a double-layer linear taper waveguide of a length of 50 μm is incorporated for mode transition between the strip and rib waveguides.

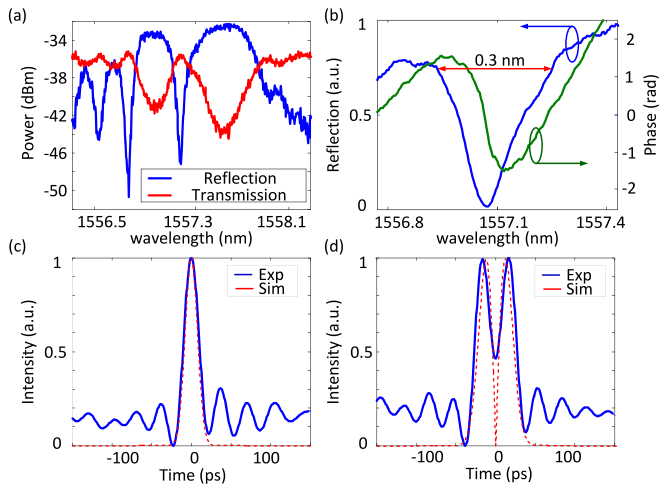

Fig. 3. (a) Measured reflection and transmission spectral responses of the fabricated PS-WBG on a rib waveguide. (b) Zoom-in view of the reflection notch and its phase response. (c) An input Gaussian pulse with an FWHM of 25 ps. (d) Temporally differentiated pulses by simulation and experiment. [33].

The PS-WBG was fabricated using a CMOS-compatible process with 248-nm deep ultraviolet lithography. Fig. 2(c) is an image of the fabricated PS-WBG captured by a microscope camera. Fig. 2(d) shows a zoom-in view of the grating couplers and the strip waveguides, and Fig. 2(e) shows a zoom-in view of the taper waveguides for mode transition between a strip waveguide and a rib waveguide. Optical performance evaluation of the fabricated PS-WBG was performed. Fig. 3(a) shows the reflection and transmission spectra of the fabricated PS-WBG. As can be seen, a resonant transmission window is located within the stop band in the transmission spectrum. Fig. 3(b)

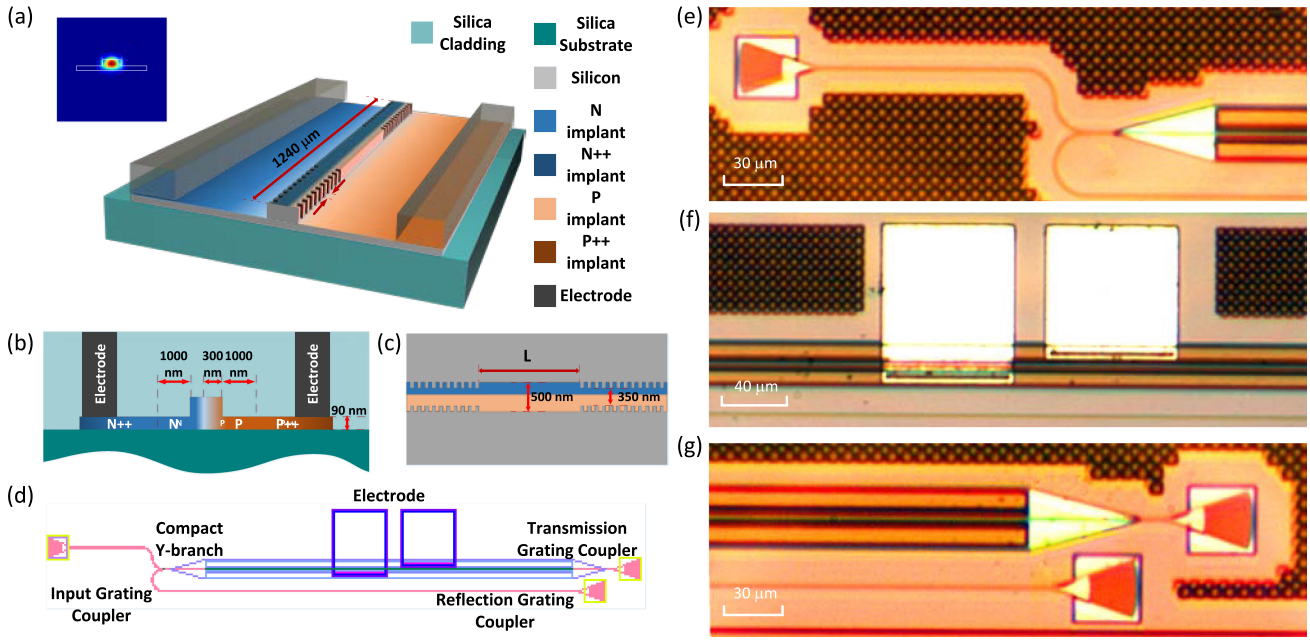

Fig. 4. (a) Perspective view of an electrically tunable PS-WBG. (Inset: Simulated fundamental TE mode profile of the rib waveguide) (b) Cross-sectional view of the PS-WBG. (c) Top view of the FP cavity. (d) Schematic layout of the PS-WBG. (e) Image of the input grating coupler. (f) Image of the electrodes. (g) Image of the transmission and reflection grating couplers in the fabricated PS-WBG. [39].

shows the width of the reflection notch (top-to-top width) of the fabricated PS-WBG, which is approximately 0.3 nm (or 37.5 GHz). The phase response shows a phase jump of π at the Bragg wavelength, which is important for the implementation of a temporal differentiator.

The PS-WBG was used for signal processing. Specifically, the PS-WBG was used to implement an all-optical temporal differentiator. As one of the basic processing blocks, an all-optical temporal differentiator is used to perform temporal differentiation of the complex envelope of an arbitrary optical waveform, which can find applications in ultra-fast signal processing [34], [35], pulse shaping [36], [37], and pulse coding [38]. Fig. 3(c) shows an experimentally generated Gaussian pulse (blue-solid line) as an input signal. An ideal Gaussian pulse (red-dashed line) is also shown for comparison. The ripples observed at the tails of the experimentally generated Gaussian pulse are resulted from the limited sampling rate of the waveform generator. Since the phase jump is π, it is a first order temporal differentiator. Fig. 3(d) shows the temporally differentiated pulse (blue-solid line) generated using the PS-WBG. The simulated temporally differentiated pulse (red-dashed line) is also shown. As can be seen, the experimentally generated pulse is close to the simulated pulse, which confirms effectiveness of the use of the PS-WBG to perform temporal differentiation. Same ripples are observed in the experimentally generated pulse, and the dip in the center of the experimentally differentiated pulse is not as deep as the simulated pulse, which are mainly caused by the limited bandwidth of the photodetector. The key advantage when using a silicon-based PS-WBG to realize a photonic temporal differentiation is that the PS-WBG has a compact size and a higher fabrication tolerance, and holds a significant potential for full system integration.

The key problem associated with a PS-WBG is that once the grating is fabricated, it can hardly be tuned, which heavily limits its application. For example, to make a tunable temporal differentiator, the phase response of the PS-WBG is required to be tuned in a large range. To address this issue, the effect of free-carrier plasma dispersion in silicon can be employed to realize the tuning of a grating. In addition, the tuning speed is ultra-fast, in the order of nanoseconds, much faster than thermal tuning, which is highly needed for ultra-fast signal processing.

Based on this concept, an electrically tunable PS-WBG on a silicon photonic chip was implemented, in which the cladding layer of silica was removed in order to clearly illustrate the internal structure of the device [39]. The inset in Fig. 4(a) shows a simulated mode profile of the fundamental TE mode at 1550 nm. To increase the tuning efficiency, an asymmetrical lateral PN junction was employed to enable electrical tuning of the grating based on the plasma dispersion effect. As shown in Fig. 4(b), the PN junction was slightly shifted to the left from the center of the waveguide by 50 nm, to increase the mode overlap with the p-type doping region, since the plasma dispersion effect is more sensitive to the change of the free-hole concentration than the free-electron concentration. Additional p^{++} and n^{++} implantations, 1 μm away from the rib to minimize absorption losses, were posed for ohmic contact formation. Fig. 4(c) provides the top view of the grating structure on the rib and the Fabry-Perot (FP) cavity. The periodic sidewall corrugations with a depth of 75 nm were introduced to the rib. To enable the device to work in the C band, the grating period is designed to be 310 nm with a duty cycle of 50%, and the FP cavity, with a length L of 24.025 μm, is allocated at the center of the grating. Fig. 4(d) shows the schematic layout of the device. Two contact windows

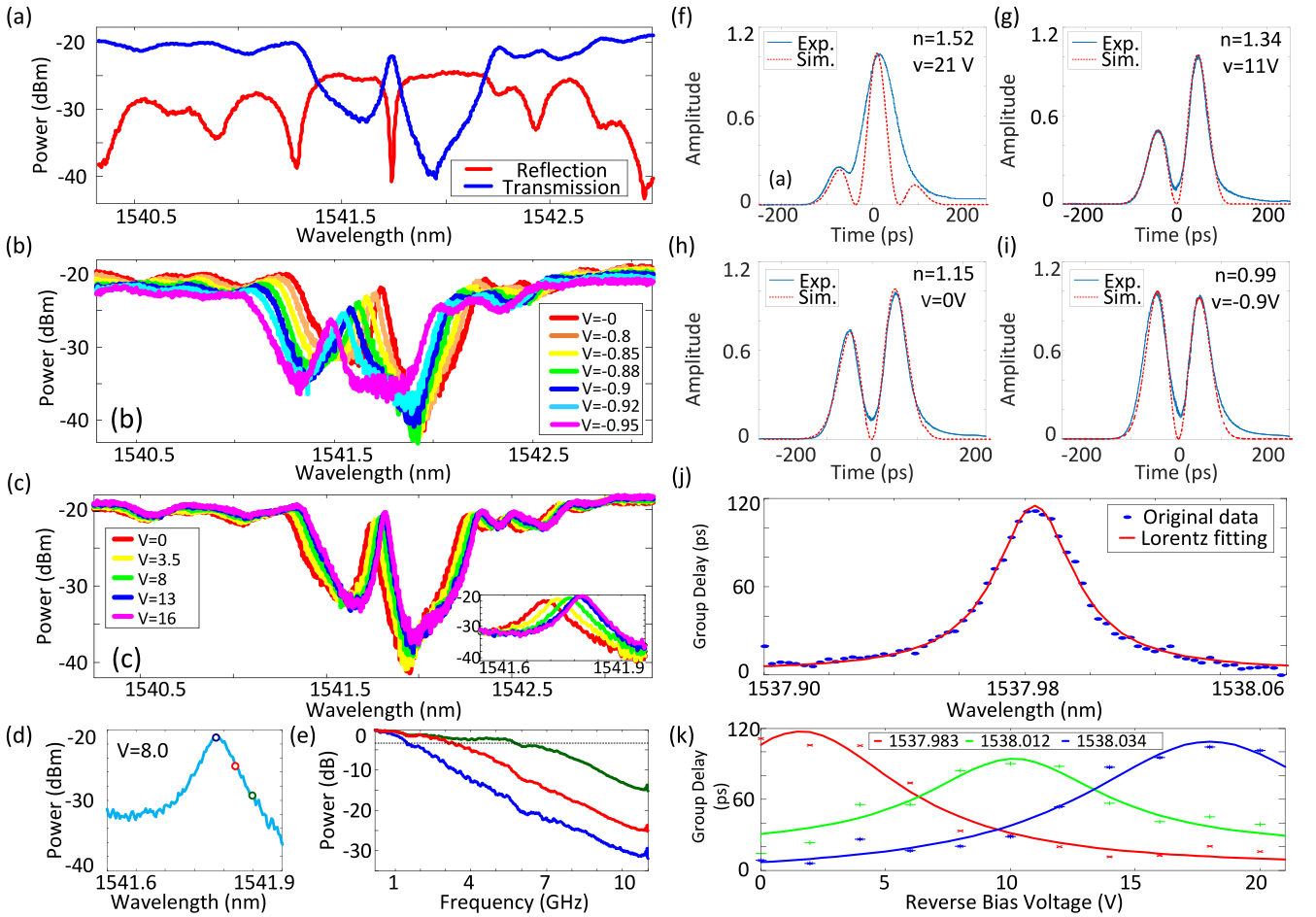

Fig. 5. (a) Measured reflection and transmission spectra of the tunable PS-WBG with a zero bias voltage applied. (b) Wavelength shift of the transmission spectrum when forward biased. (c) Wavelength shift of the transmission spectrum when reverse biased (Inset: Zoom-in view of the wavelength shift of the transmission window). (d) Measured transmission window of the PS-WBG when reverse biased with a voltage of 8.0 V. (e) Measured frequency responses for three different wavelengths when the reverse bias voltage is 8.0 V. (f)-(i) Temporal differentiation results with the differentiation order tuned. (j) Measured group delay response in the notch of the fabricated PS-WBG. (k) Electrical tunability of the group delay at three different wavelengths. [39], [40].

are opened on the silica pads, with 2-μm-thick aluminum layer deposited to make the contacts.

The device was fabricated using a CMOS-compatible process with 248-nm deep ultraviolet lithography. Fig. 4(e) is an image of the input grating coupler in the fabricated PS-WBG, captured by a microscope camera. At front end of the PS-WBG, there is a taper waveguide to achieve the mode conversion and a compact-Y branch to split the reflected light signal to the reflection grating coupler. Fig. 4(f) is an image of the electrodes in the fabricated PS-WBG. A bias voltage from a DC power supply is applied via an electrical probe to the PN junction to achieve spectral tuning. Fig. 4(g) is an image of the transmission and reflection grating couplers in the fabricated PS-WBG. Again, there is a taper waveguide at the rear end of the PS-WBG to achieve mode conversion. Spectral measurement in Fig. 5(a) shows that the notch in the reflection band has approximately 46 pm with a Q-factor of 33,500, and an extinction ratio is 16.4 dB. DC performance of the PS-WBG in Fig. 5(b) and (c) shows that the average central wavelength shift rates for a forward and reverse bias are -1.15 nm/V and 4.2 pm/V, respectively. Since the light confining resonating structure of the FP cavity can enhance the effect of refractive index change, the electrically tunable can be employed as an electro-optic modulator. Fig. 5(d) shows the transmission window of the PS-WBG when a reverse-bias voltage of 8.0 V is applied, and three circles are used to indicate the different input wavelengths. Fig. 5(e) shows the electro-optic frequency response for the three different input wavelengths. As can be seen, the maximum 3-dB modulation bandwidth is 5.6 GHz, and with the wavelength of the input light further away from the resonance wavelength, the measured 3-dB modulation bandwidth is becoming larger.

Fast electrical tuning speed and large tuning range make the tunable PS-WBG very suitable for photonic processing of microwave signals such as frequency-tunable microwave filtering, fractional-order tunable temporal differentiation, Hilbert transformation and true time delay [40]. For example, by using the fabricated tunable PS-WBG, a fractional-order tunable temporal differentiation was implemented. Fig. 5(f)–(i) shows the temporally differentiated pulses (blue-solid line) with differentiation orders of 1.52, 1.34, 1.15, and 0.99, respectively, when the PS-WBG is biased at different voltages as a temporal differentiator. The simulated output pulses with an ideal Gaussian pulse as

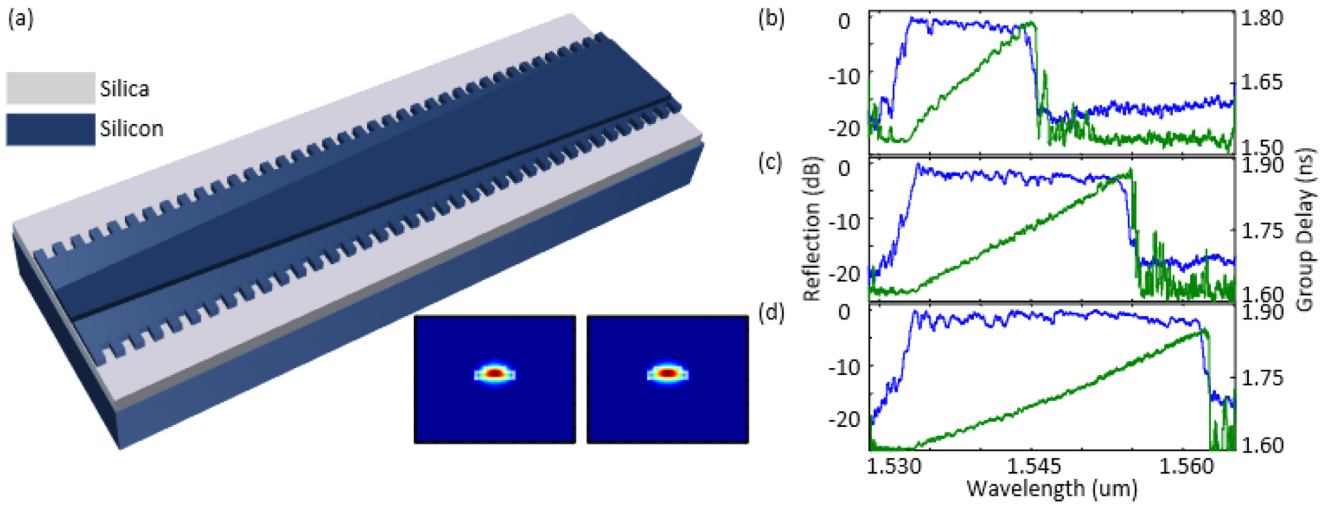

Fig. 6. (a) Perspective view of an LC-WBG. (Inset: Simulated fundamental TE mode profile of the rib waveguide with the rib width of 500 nm (left) and 650 nm (right)). Measured spectral and group delay responses of an LC-WBG with the rib width linearly increasing from 500 to (b) 550 nm, (c) 600 nm, and (d) 650 nm. [41].

an input optical signal to an ideal differentiator with the same orders are also shown (red-dashed line) for comparison. As can be seen, the experimentally generated pulses are close to the simulated pulses, which confirms the effectiveness of the use of the tunable PS-WBG to perform a tunable fractional-order differentiator. Again, the slight mismatch in the dip is mainly caused by the limited bandwidth of the photodetector. We may note, since the notch wavelength is shifted with different bias voltages, the wavelength of the input optical signal is required to be tuned, which largely increase the implementation complexity. Therefore, a tunable fraction-order temporal differentiator with a fixed resonance wavelength is highly needed.

In addition, due to a strong light-confinement capacity of the optical cavity between the two reflectors (gratings) in the PS-WBG, the PS-WBG has a strong dispersion near the center of the notch and thus a large group delay, which could be used as an optical true time delay line. By tuning the bias voltage, the notch center and the phase response are tuned, which would produce a tunable optical delay line. Fig. 5(j) illustrates the measured group delay response in the notch in the fabricated PS-WBG. The PS-WBG has a group delay as large as 110 ps at the notch center. Fig. 5(k) shows the electrical tunability of the group delay at three different wavelengths. As the bias voltage is increasing, the group delay is changed. For example, at 1538.012 nm, shown in the red line, as the bias voltage increases, the time delay is firstly increased to 95 ps from 32 ps at a bias voltage of 0 V and then is decreased to 35 ps when the bias voltage is 21 V.

The key advantage of using an electrically tunable PS-WBG for microwave signal processing is its ultra-fast tuning speed of a few nano-seconds. However, the main disadvantage is its narrow bandwidth. For applications such as true time delay lines, wide bandwidth is always required. To increase the bandwidth, a solution is to use a linearly chirped waveguide Bragg grating (LC-WBG) [41]. Fig. 6(a) shows the perspective view of a LC-WBG, which is realized by introducing sidewall corrugations on the slab, by linearly increasing the width of the rib along the grating while keeping the grating period uniform, a linear chirp is produced since the effective refractive index is linearly increasing as the rib width increases in a definite range. The inset in Fig. 6(a) shows the simulated fundamental TE mode profiles in a rib waveguide with a rib width of 500 nm (left) and 650 nm (right).

TABLE I
PROPERTIES OF LC-WBGS*

Rib Width (nm)	Bandwidth (nm)	Delay (ps)	Dispersion (ps/nm)	Chirp Rate (nm/mm)
550	1533~1544	228	20.7	0.88
600	1534~1554	236	11.8	1.59
50	1533~1562	241	8.3	2.31

*Each LC-WBG has a linearly increasing rib width starting from 500 nm.

The LC-WBG was fabricated using a CMOS-compatible process with 193-nm deep ultraviolet lithography. Fig. 7(a), (b) and (c) show the measured reflection spectrum in blue and the group delay in green of the fabricated LC-WBG with the rib width linearly increasing from 500 to 550 nm, 500 to 600 nm, and 500 to 650 nm, respectively. As can be seen, by controlling the rib width, it is convenient to tailor the reflection response and the chirp rate of an LC-WBG. Table I presents the reflection bandwidth, time delay, dispersion and chirp rate of each of the LC-WBGs in Fig. 7. The simplicity in tailoring the spectrum and the chirp rate enables an LC-WBG to be designed in satisfying specific requirements for applications such as an optical delay line, which should have a broad bandwidth and a comparatively small optical transmission loss.

However, the LC-WBG shown in Fig. 7 is not tunable. To enable the LC-WBG to be electrically tunable, a lateral PN junction is introduced to the grating, which is used to tune the grating due to the plasma dispersion effect [42]. Fig. 7(a) presents the top view of the electrically-tunable LC-WBG. To effectively suppress the sidelobes in the reflection spectral response, Gaussian apodization, a technique widely used to tailor

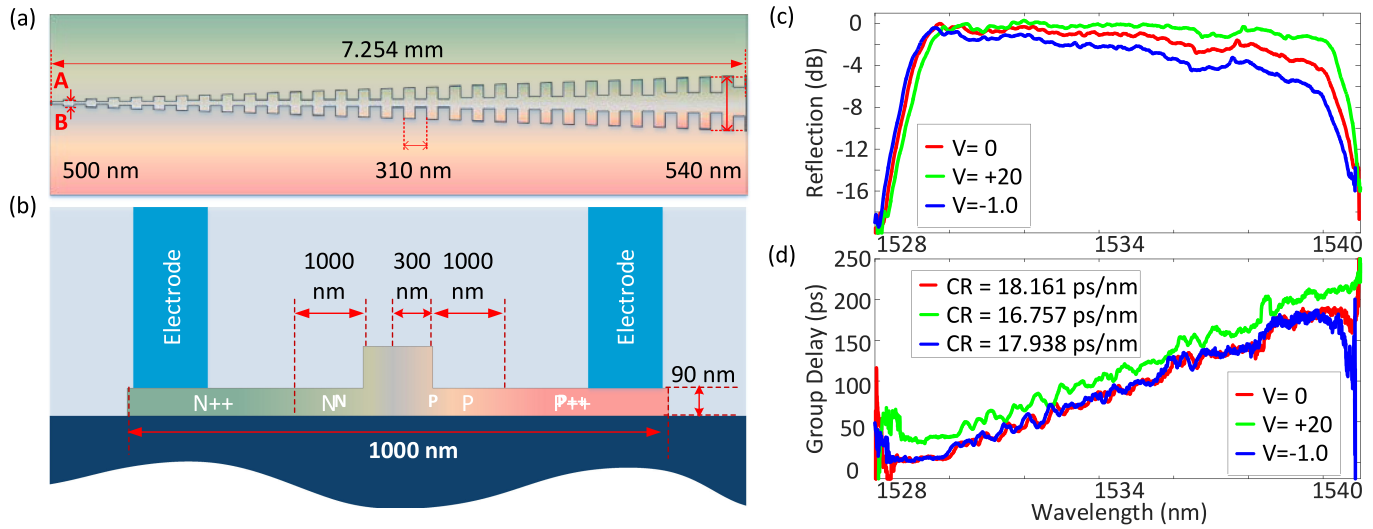

Fig. 7. (a) Top-view of the electrically-tunable LC-WBG. (b) Cross-section view of the electrically tunable LC-WBG along the line AB. (c) Measured spectral and (d) group delay responses of a fabricated electrically-tunable LC-WBG under the different bias voltages. [42].

the grating spectral response to reduce the sidelobes, is applied to the grating, which is done by varying the corrugation depths in a raised Gaussian profile along the rib waveguide. Fig. 7(b) presents the cross-sectional view of the electrically-tunable LC-WBG along the line AB in Fig. 7(a). Again, an asymmetrical lateral PN junction was employed, which is slightly shifted to the left from the center of the waveguide by 50 nm. Such a shift could increase the mode overlap with the p-type doping region to achieve a higher tuning efficiency, since the plasma dispersion effect is more sensitive to the change of the free-hole concentration.

The electrically-tunable LC-WBG was fabricated using the CMOS-compatible process with 248-nm deep ultraviolet lithography. Fig. 7(c) and (d) shows the normalized reflection spectral and group delay responses of the LC-WBG when it is biased at 0 V, +20 V and −1.0 V, respectively. When the bias voltage is zero, as shown in Fig. 7(c) and (d) in red, the grating exhibits a time delay of 174.9 ps between 1529.14 and 1538.77 nm and thus has a dispersion value of 18.2 ps/nm and a chirp rate of 1.328 nm/mm. Note that the grating has a comparatively large insertion loss at the longer wavelength. This is because the light wave with a longer wavelength needs to travel a longer distance in the LC-WBG until it is reflected at the right location of the LC-WBG, since the rib width is linearly increasing along the grating. The loss includes the grating-induced loss and the doping-induced loss. When the grating is forward biased at −1.0 V, as shown in Fig. 7(c) and (d) in blue, the grating exhibits a time delay of 124.10 ps between 1529.10 and 1536.00 nm and thus has a dispersion value of 17.9 ps/nm and a chirp rate of 0.951 nm/mm. Compared to the spectrum at the zero bias, the spectrum is slightly blue-shifted. For forward biasing, when the bias voltage is increasing, the free-carrier injection would decrease the refractive index due to the plasma dispersion effect, which leads to a blue shift in the spectrum. In the meanwhile, the increased free-carrier density would also introduce an excess absorption loss. Therefore, the blue line exhibits a clearly changing insertion loss for different wavelengths. When the grating is reversed biased at +20 V, as shown in Fig. 7(c) and 7(d) in green, the grating exhibits a time delay of 182.27 ps between 1529.36 and 1540.24 nm and thus has a dispersion value of 16.8 ps/nm and a chirp rate of 1.500 nm/mm. Again, a red-shift in the spectrum is observed. For reverse biasing, when the bias voltage is increasing, the free-carrier extraction would increase the refractive index via plasma dispersion effect, which leads to a red shift in the spectrum. Furthermore, since the free-carrier density is decreased, the doping-induced loss is decreased, which would alleviate the insertion loss difference for the light wave at different wavelengths. As can be found Fig. 7(c) and (d), the magnitude and group delay responses of the LC-WBG could be tuned by controlling the bias voltage, which is a potential solution to act as an electrically tunable optical delay line. Note that the ripples in the magnitude and the group delay responses are high, which are mainly caused by the fabrication limitations since the line width of the corrugations is smaller than the feature size. To reduce the ripples, advanced fabrication process should be used, in which the feature size should be smaller than the minimum line width of the LC-WBG. In addition, by applying an optimized apodization to the grating profile, the ripples could also be reduced.

Although the grating spectral response could be tuned based on the free-carrier plasma dispersion effect in silicon, these tuning are mainly limited to shifts of the center wavelength. For many applications, other spectral characteristics, such as spectral shape and phase response, are required to be tunable. For example, with the explosive growth of data traffic, the elastic optical network (EON) architecture is considered a promising solution for next-generation optical networks [43]. Distinct from that in current optical networks, the spectrum grid in an EON is flexible. To address the need for flexible division of the optical spectrum, a reconfigurable optical add-drop multiplexer is an essential component, which can generate elastic optical paths by reconfiguring its filter response [44]. A programmable grating

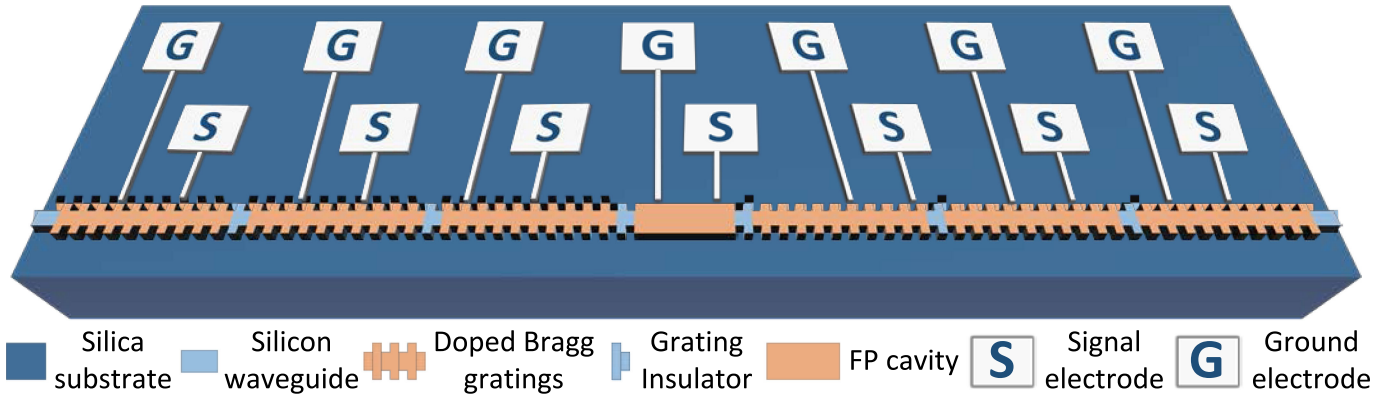

Fig. 8. Schematic view of the programmable grating. A pair of electrodes (Signal and Ground) are connected to each independent PN junction for controlling. [26].

filter is a strong candidate to fulfill this role. By controlling bias voltages, the grating spectral response can be reconfigured to fit into different applications [26].

IV. Programmable Bragg Gratings

A programmable grating that can be flexibly reconfigured was designed and demonstrated, as shown in Fig. 8. The grating consists of multiple series-connected uniform Bragg grating sections, in which the gratings are produced by creating periodic corrugations on the rib sidewall, and a Fabry-Pérot (FP) cavity section in the middle of the grating. Each uniform Bragg grating section incorporates an independent lateral PN junction, and between two neighboring sections there is an un-doped grating to function as an electrical insulator. Distributed electrodes are connected to the independent PN junctions. By applying a bias voltage to a PN junction, the refractive index of the grating in that particular section could be tuned locally based on the free -carrier plasma dispersion effect. Thus, the entire index modulation profile of the grating could be electrically reconfigured by field programming all the bias voltages, which enables the grating to have diverse spectral characteristics for diverse applications.

The programmable grating was again fabricated in a CMOS-compatible process using 248-nm deep ultraviolet lithography. Fig. 9 shows the chip image, in which the grating has a symmetrical configuration, consisting of two identical uniform sub-grating sections (left and right) and a FP cavity section in the middle. Each section has an independent PN junction for local tuning. Three grating couplers are used to couple light between the chip and the input and output fibers, and a compact Y-branch is used to collect the reflected light. Fig. 9(a) shows the microscope camera image of the fabricated programmable grating with a length of 1.560 mm and a width of 0.196 mm. Fig. 9(b)–(f) gives zoomed-in views of the input grating coupler and the compact Y-branch, the transmission and reflection grating couplers, the left sub-grating section, the FP cavity section, and the right sub-grating section, respectively. Since the local refractive index in each particular section could be tuned by applying a bias voltage to the PN junction across the section, by field programming three bias voltages, the index modulation profile of the grating can be reconfigured, and thus the grating spectral characteristics can be tailored.

The programmable grating can be reconfigured to be different gratings. First, a phase-shifted waveguide Bragg grating is implemented by introducing a phase shift in the middle of a uniform grating. For the fabricated programmable grating, the phase shift is realized by the FP cavity. Fig. 10(a) shows the measured reflection and transmission spectra of the fabricated grating in the static state. As can be seen, a resonant window is located within the stopband in the transmission spectra (in red), which is a distinct feature of a phase-shifted Bragg grating.

Fig. 10(b) shows a zoomed-in view of the notch wavelength shift in the reflection band when two bias voltages applied to the PN junctions in the left and right sub-grating sections vary synchronously. Thanks to the free-carrier plasma dispersion effect, the free-carrier concentration in the waveguide introduces a change in the refractive index, which leads to the shift of the Bragg wavelength. Fig. 10(c) shows the tuning of the extinction ratio while the notch wavelength is maintained unchanged for different bias voltage combinations. As demonstrated in the electrically tunable PS-WBG, it is not possible to tune the notch extinction ratio while maintaining the notch wavelength unchanged. In the fabricated programmable grating, by field programming the three bias voltages, the notch wavelength shifts induced by the PN junctions could counteract. Thus, the notch wavelength can be preserved, while different bias voltage combinations could lead to a different roundtrip loss, which would result in a different notch extinction ratio.

In addition, the fabricated grating can be reconfigured as a uniform grating, which is realized by failing the optical confinement capability of the FP cavity, by applying a large forward bias voltage to the right PN junction. Fig. 10(d) gives the measured spectra of the grating when a large forward bias voltage is applied to the right PN junction. The large forward bias voltage enables the injection of massive free-carriers into the waveguide, which would cause a heavy optical absorption loss and thus disable the reflection capability of the right sub-grating. As can be seen, there is one main peak in the reflection or a notch in the transmission spectrum, which is a distinct feature

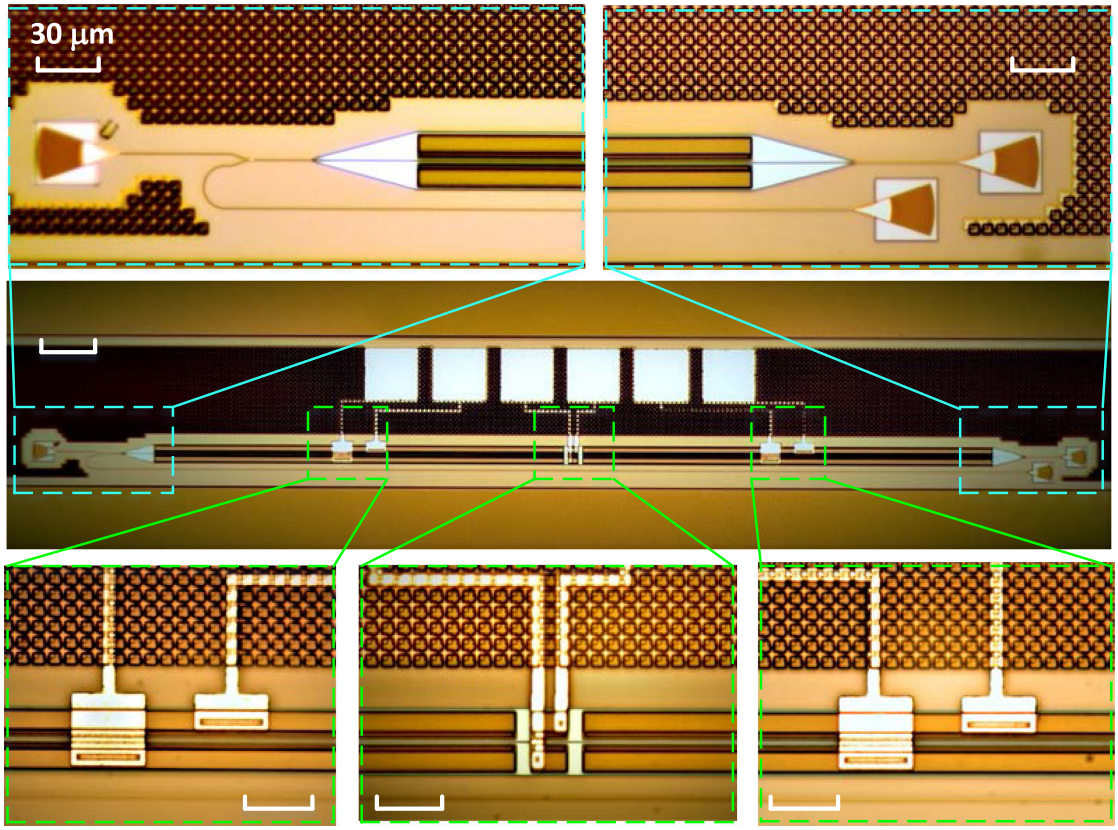

Fig. 9. Microscope camera images of the fabricated programmable grating. (a) Entire grating. (b) Input grating coupler and compact Y-branch. (c) Transmission and reflection grating couplers. (d) Left sub-grating section. (e) FP cavity section. (f) Right sub-grating section. [26].

of a uniform grating. In addition, by tuning the bias voltage applied to the PN junction in the left sub-grating section, the center wavelength of the uniform grating could be tuned, as shown in Fig. 10(e). There is another approach to reconfigure the fabricated grating to be a uniform grating, which is realized by applying a large forward bias voltage to the cavity PN junction. Fig. 10(f) gives the measured spectra of the uniform grating when a forward bias voltage is applied to the cavity PN junction. A large forward bias voltage enables the injection of a massive quantity of free-carriers into the cavity to cause a heavy optical absorption loss. Therefore, by programming voltages applied to the PN junctions, the fabricated grating could present some uncommon optical characteristics which are difficult to achieve by using a conventional grating. This is a unique feature of the programmable grating. Since the PN junctions in the left and right sub-grating sections can be independently controlled, the uniform sub-gratings in the two sections could be tuned independently. Fig. 10(g) gives the measured spectra of two uniform sub-gratings when a reverse bias voltage is applied to the left PN junction, and a forward bias voltage is applied to the right PN junction. Thus, the left sub-grating is red shifted and the right sub-grating is blue shifted, which reconfigures the fabricated grating to be two nonidentical uniform sub-gratings. As can be seen, there are two separate main reflection peaks in the reflection spectra. Additionally, the ability to independently tune (and thereby shift the spectral response of) the left and right uniform sub-gratings, enables the device to be reconfigured as a chirped grating. Fig. 10(h) presents the measured spectra of the chirped grating when a maximum reverse bias voltage is applied to the left PN junction and a forward bias voltage is applied to the right PN junction. As observed, the 3-dB bandwidth of the spectra is increased largely, which is much larger than that of the uniform grating. By increasing the grating length and dividing the grating into more sections, the grating would have a better optical performance in terms of the group delay and chirp rate.

The programmable grating can find numerous applications. An application example is its use for programmable signal processing, in which three signal processing functions including temporal differentiation, true time delay, and microwave frequency identification have been demonstrated [26]. In fact, a programmable microwave signal processor based on a programmable grating could perform other signal processing functions such as microwave filtering, temporal integration, and Hilbert transformation. In addition to its use in microwave signal processing, the programmable grating could also be employed for arbitrary microwave waveform generation. For example, it can be used as a spectral shaper to generate a chirped microwave waveform for radar and other imaging applications. An array of such gratings can also be used as a beamforming network to generate true time delays for wideband squint-free beam steering. By increasing the number of independent sub-grating

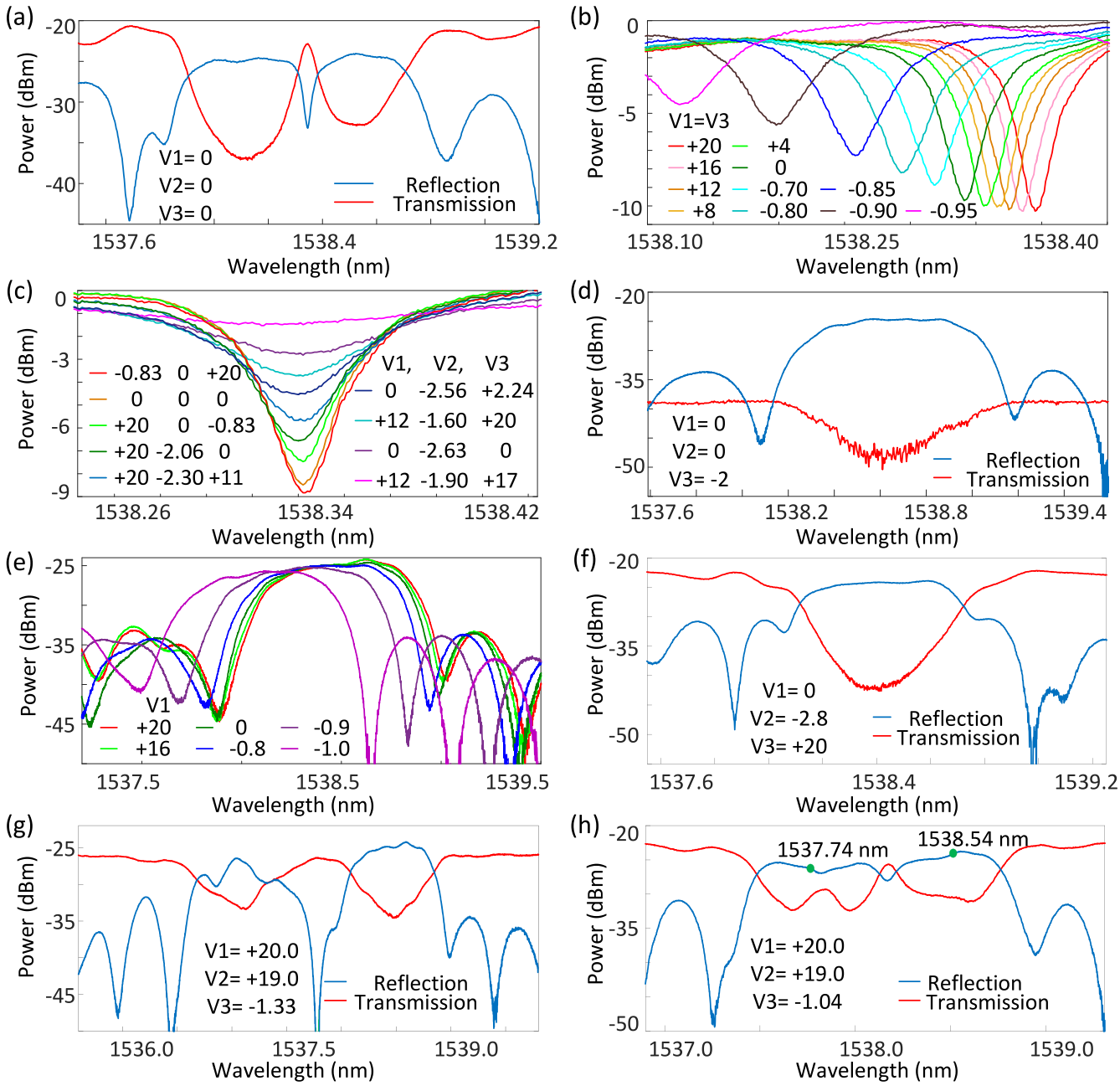

Fig. 10. Measured reflection and transmission spectra. (a) Spectra of the fabricated grating in the static state. (b) Notch wavelength shift when the bias voltages applied to the left and right sub-gratings vary synchronously. (c) Extinction ratio tuning while the notch wavelength is kept unchanged. (d) Spectra when the grating is reconfigured to be a uniform grating. (e) Wavelength tuning of the uniform grating. (f) Spectra when the device is reconfigured to be a uniform grating by increasing the cavity loss. (g) Spectra when the device is reconfigured to be two independent uniform sub-gratings. (h) Spectra when the device is reconfigured to be a chirped grating. [26].

sections, the functionalities of the signal processor could be further increased, and the performance could be enhanced.

V. Equivalent Phase Shifted Bragg Gratings

The key to implement the programmable grating is to introduce an accurate phase shift, which is a quarter of the Bragg wavelength, and thus a stringent fabrication accuracy is required to make an accurate phase shift. The major limitation in implementing a phase-shifted Bragg grating on silicon is the poor spectral accuracy due to the poor fabrication tolerance. To have a precise spectral response, high precision lithography must be used, but it is not available at this moment. To implement a Bragg grating having a precise spectral response without using high-precision lithography, a solution is to use the equivalent-phase-shifted (EPS) grating technique [45]. An equivalent phase shift can be achieved based on nonuniform spatial sampling of a uniform Bragg grating. By controlling the sampling profile, a high-precision EPS Bragg grating with different spectral response can be achieved [46], [47]. Since the sampling period is in

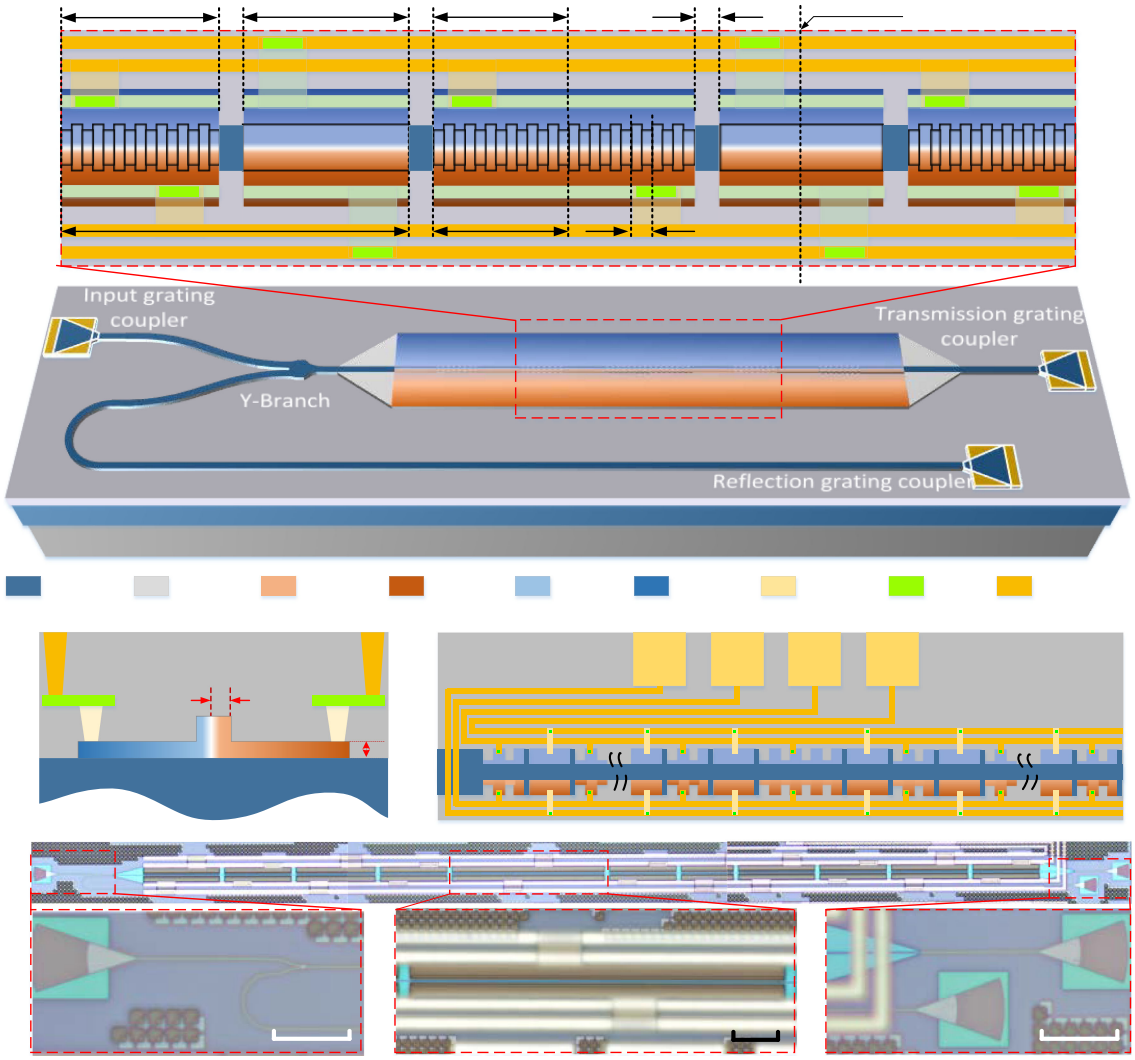

Fig. 11. (a) Perspective view of the programmable EPS waveguide Bragg grating on a silicon photonic chip. (b) Zoom-in view of the grating structure. (c) Cross-section view of the waveguide with doping in the grating. (d) Top-view of the designed EPS Bragg grating. (e) Image of the entire programmable EPS grating. (f) Image of the input grating coupler. (g) Image of the increased sampling period ΔL. (h) Image of transmission and reflection grating couplers. [27].

micrometer range while the grating pitch is in nanometer range, a requirement for fabrication accuracy is reduced by three orders of magnitude as compared with the conventional fabrication technique. Recently, an EPS waveguide grating on silicon was demonstrated [48], [49]. Since the sampling profile was fixed, the spectral response was fixed and could not be tunable.

By introducing PN junctions to an EPS waveguide Bragg grating, the grating can be made programmable. Fig. 11(a) illustrates the schematic of a programmable EPS waveguide Bragg grating on a silicon photonic chip [27]. Fig. 11(b) gives a zoom-in view of the grating, which is produced by creating the periodic corrugations on the waveguide sidewall. An equivalent phase shift is realized by spatially sampling a uniform grating to create an increased sampling period $P + \Delta L$ in the center for the grating, where P is spatial sampling period and ΔL is the sampling period increment. In the design, the sampling period increment is selected to be $\Delta L = P/2$, which leads to an odd integer number of π phase shift to the odd-order channels. Considering the sampling period P is three orders of magnitude larger than the grating pitch Λ, the requirement for lithography accuracy would be highly reduced. In addition, by manipulating the sampling period P, a new degree of freedom in the grating design is enabled, which offers the flexibility in producing a grating with arbitrary spectral response. To make the grating electrically programmable, independent lateral PN junctions are incorporated along the grating. As shown in Fig. 11(b), in a sampling period, two independent PN junctions are distributed in the on-modulation grating section and off-modulation grating section. To avoid mutual electrical coupling between neighboring PN junctions, a section of undoped waveguide is used as an electrical insulator. Fig. 11(c) shows the cross-sectional view of the lateral PN junction along the dashed line AA' in Fig. 11(b). Fig. 11(d) gives the top-view of the EPS Bragg grating. In our design, the entire device has 11 sampling periods in total. In the whole EPS Bragg grating, all the PN junctions in the on-modulation grating sections are connected and share

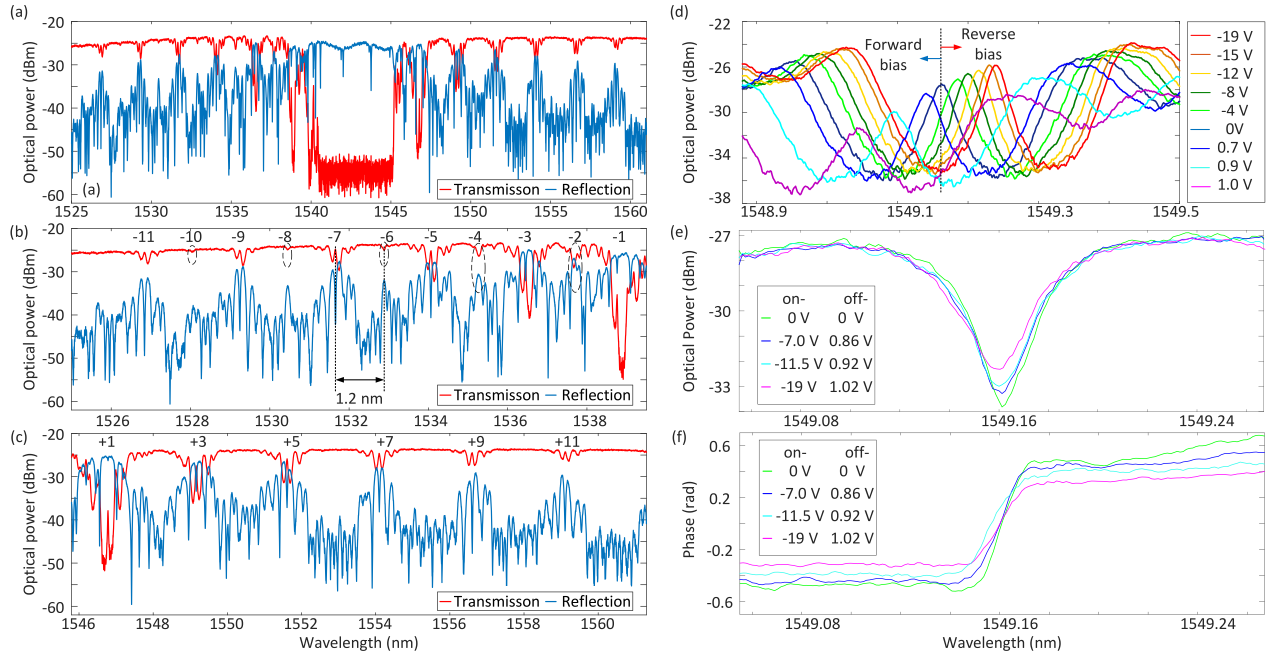

Fig. 12. (a) Measured reflection and transmission spectra of the EPS Bragg grating. (b) Zoom-in view of the reflection and transmission spectra of the negative-order channels. (c) Zoom-in view of the reflection and transmission spectra of the positive-order channels. (d) Transmission window peak wavelength shifting and its power variation when the PN junctions are biased. (e) Tuning of the extinction ratio of the reflection notch in the $+3^{rd}$ channel with the notch wavelength kept unchanged. (f) Tuning of the phase jump of the reflection notch in the $+3$rd channel. [27].

one pair of the electrical contacts, and all the off-modulation grating sections are connected and share another pair of the electrical contacts. Thus, by controlling the bias voltages for the on-modulation grating sections and the off-modulation grating sections, the grating pitch Λ, the sampling length P and the sampling period increment could be tuned, which provides full reconfigurability of the EPS Bragg grating. The key advantages of the programmable ESP Bragg grating include largely reduced requirements for fabrication accuracy and significantly increased tuning capability.

The programmable EPS Bragg grating was fabricated in a CMOS-compatible process using 193-nm deep ultraviolet lithography. Fig. 11(e) is an image of the entire grating captured by a microscope camera. Fig. 11(f) shows a zoom-in view of the input grating coupler. Fig. 11(g) provides an image of the increased sampling period in the center of the EPS Bragg grating. The sampling period increment ΔL is chosen to make an odd integer number of π phase shift in the odd-order channels. Fig. 11(h) gives an image of the transmission and reflection grating couplers. Compared with a conventional phase-shifted Bragg grating, the EPS Bragg grating is markedly advantageous in terms of implementation flexibility, repeatability, and cost-effectiveness, which are highly suitable for mass production. These features become more important when multiple and variable phase shifts are needed. In addition, the availability of phase shift tuning via electrically tuning the distributed PN junctions gives a new degree of freedom in the spectrum tuning, which is useful for programmable signal processing.

Fig. 12(a) shows the measured reflection and transmission spectra of the fabricated EPS Bragg grating in the static state. The red line shows the measured transmission spectrum, while the blue line shows the measured reflection spectrum. Thanks to the spatial sampling, the grating has a multichannel reflection and transmission spectra. Due to the equivalent phase shift caused by the increased sampling period, in the odd-order channels, a passband in the transmission stopband and a notch in the reflection passband are observed, which are the typical spectral features of a phase-shifted Bragg grating and confirms the effectiveness of the EPS approach in the implementation of a phase-shifted Bragg grating. Fig. 12(b) shows the reflection and transmission spectra of the negative-order channels. As can be seen, only the odd-order channels have EPS-resulted spectral features, while the even-order channels have spectral responses that are not affected by the EPS. This is understandable because all even-order channels would have a phase shift that is an integer number of 2π. Thanks to the strong index modulation of the waveguide grating, the 11th channel spectral response could still be seen. Fig. 12(c) shows the reflection and transmission spectra of the positive order channels. The spectral responses of the odd-order channels with EPS-resulted spectral features are clearly seen, while the spectral responses of the even-order channels disappear, which, again, is due to the coupling of the even-order modes into the cladding. As a distinct feature of an EPS Bragg grating is that multichannel phase shifts could be introduced, which offers the possibility for simultaneous manipulation of multiple wavelengths, thus increasing the capability of the grating for programmable multichannel signal processing. For example, an EPS Bragg grating with well controlled channel spacing can be employed in a WDM system for advanced multichannel signal processing [50], [51].

By field programming the bias voltages, the grating could be electronically reconfigured. When the two bias voltages are simultaneously and synchronously changed from -19 to $+1$ V, the grating spectrum would be shifted. Fig. 12(d) shows the measured reflection and transmission spectra of $+3^{rd}$ channel in the grating. For the PN junctions being reverse biased, the spectrum is red shifted; while, for the PN junctions being forward biased, the spectrum is blue shifted. Since the PN junctions in the on-modulation and off modulation grating sections can be independently controlled, the spectrum shift induced by each junction could cancel each other. Thus, the resonant wavelength can be maintained unchanged, while the extinction ratio and phase jump of the reflection notch can be changed. Fig. 12(e) shows the tuning of the extinction ratio while the notch wavelength is maintained unchanged for different bias voltage combinations. By field programming the bias voltages, the notch wavelength shifts induced by the on and off-modulation grating sections can counteract. Thus, the notch wavelength can be kept unchanged, while different bias voltage combinations could lead to a different loss, which leads to a different extinction ratio. As shown in Fig. 12(e), the extinction ratio is changed from 6.4 to 4.5 dB. Fig. 12(f) shows the phase response of the reflection notch in the $+3^{rd}$ channel. As can be seen, by programming the bias voltages, the phase jump at the notch center can be tuned from 1.0 to 0.48. The tuning range could be increased by independently controlling all the PN junctions in the grating.

VI. Conclusion

An overview of our recent work on silicon-based waveguide Bragg gratings and the applications was presented, with an emphasis on programmable waveguide Bragg gratings and their use for high-speed photonic signal processing. Silicon photonics provides an excellent platform for the grating implementations since it leverages the mature CMOS technology with a high yield and a low cost. Moreover, it is a promising platform to integrate waveguide gratings with other photonic devices on a single chip. As the performance of high-speed and high-efficient silicon modulators and on-chip Germanium photodetectors is keeping improving, especially hybrid solutions to heterogeneously integrate III-V materials onto silicon photonic platform to overcome the key challenge in producing light sources and amplifiers, a promising prospect to realize full system-level integration is coming.

Acknowledgment

The authors would like to thank CMC Microsystems for the provision of services that have facilitated this research.

References

[1] K. O. Hill, Y. Fujii, D. C. Johnson, and B. S. Kawasaki, "Photosensitivity in optical fiber waveguides: Application to reflection filter fabrication," *Appl. Phys. Lett.*, vol. 32, pp. 647–649, Aug. 1978.

[2] H. Sakata, K. Nishio, and M. Ichikawa, "Tunable bandpass filter based on force-induced long-period fiber grating in a double cladding fiber," *Opt. Lett.*, vol. 35, no. 7, pp. 1061–1063, May 2010.

[3] W. Li, M. Li, and J. P. Yao, "A narrow-passband and frequency-tunable micro-wave photonic filter based on phase-modulation to intensity-modulation conversion using a phase-shifted fiber Bragg grating," *IEEE Trans. Microw. Theory Tech.*, vol. 60, no. 5, pp. 1287–1296, May 2012.

[4] J. Palaci *et al.*, "Tunable photonic microwave filter with single bandpass based on a phase-shifted fiber Bragg grating," *IEEE Photon. Technol. Lett.*, vol. 22, no. 19, pp. 1467–1469, Oct. 2010.

[5] Z. Pan *et al.*, "Tunable chromatic dispersion compensation in 40 Gbit/s systems using nonlinearly chirped fiber Bragg grating," *J. Lightw. Technol.*, vol. 20, no. 12, pp. 2239–2246, Dec. 2002.

[6] R. L. Lachance, S. Lelièvre, and Y. Painchaud, "50 and 100 GHz multi-channel tunable chromatic dispersion slope compensator," *Proc. OFC*, vol. 1, pp. 164–165, Mar. 2002.

[7] J. M. Lopez-Higuera, *Handbook of Optical Fibre Sensing Technology*. New York, NY, USA: Wiley, 2002.

[8] A. Othenos and K. Kalli, *Fiber Bragg Gratings: Fundamentals and Applications in Telecommunications and Sensing*. Norwood, MA, USA: Artech House, 1999.

[9] T. L. Yeo, T. Sun, K. T. V. Grattan, D. Parry, R. Lade, and B. D. Powell, "Polymer-coated fiber Bragg grating for relative humidity sensing," *IEEE Sensors J.*, vol. 5, no. 5, pp. 1082–1089, Oct. 2005.

[10] R. J. Schroeder, T. Yamate, and E. Udd, "High pressure and temperature sensing for the oil industry using fiber Bragg gratings written onto side hole single mode fiber," in *Proc. 13th Int. Conf. Opt. Fiber Sens., SPIE*, vol. 3746, pp. 42–45, Apr. 1999.

[11] J. P. Yao, "Microwave photonics," *J. Lightw. Technol.*, vol. 27, no. 3, pp. 314–335, Feb. 2009.

[12] J. Capmany and D. Novak, "Microwave photonics combines two worlds," *Nature Photon.*, vol. 1, no. 6, pp. 319–330, Jun. 2007.

[13] J. Capmany, J. Mora, I. Gasulla, J. Sancho, J. Lloret, and S. Sales, "Microwave photonic signal processing," *J. Lightw. Technol.*, vol. 31, no. 4, pp. 571–586, Feb. 2013.

[14] R. A. Minasian, "Ultra-wideband and adaptive photonic signal processing of microwave signals," *IEEE J. Quantum Electron.*, vol. 52, no. 1, Jan. 2016, Art no: 0600813.

[15] M. Hochberg and T. Baehr-Jones, "Towards fabless silicon photonics," *Nat. Photon.*, vol. 4, no. 8, pp. 492–494, Aug. 2010.

[16] W. Zhang and J. P. Yao, "Silicon-based integrated microwave photonics," *IEEE J. Quantum Electron.*, vol. 52, no. 1, Jan. 2016, Art no: 0600412.

[17] D. Tan, P. Sun, and Y. Fainman, "Monolithic nonlinear pulse compressor on a silicon chip," *Nature Commun.*, vol. 1, Nov. 2010, Art. no. 116.

[18] S. Khan, M. Baghban, and S. Fathpour, "Electronically tunable silicon photonic delay lines," *Opt. Exp.*, vol. 19, no. 12, pp. 11780–11785, Jun. 2011.

[19] K. Bédard, A. D. Simard, B. Filion, Y. Painchaud, L. A. Rusch, and S. LaRochelle, "Dual phase-shift Bragg grating silicon photonic modulator operating up to 60 Gb/s," *Opt. Exp.*, vol. 24, no. 3, pp. 2413–2419, Feb. 2016.

[20] W. Shi, V. Veerasubramanian, D. Patel, and D. V. Plant, "Tunable nanophotonic delay lines using linearly chirped contradirectional couplers with uniform Bragg gratings," *Opt. Lett.*, vol. 39, no. 3, pp. 701–703, Feb. 2014.

[21] E. Sahin, K. J. Ooi, C. E. Png, and D. T. H. Tan, "Large, scalable dispersion engineering using cladding-modulated Bragg gratings on a silicon chip," *Appl. Phys. Lett.*, vol. 110, no. 16, pp. 161113-1–161113-4, Apr. 2017.

[22] X. Wang *et al.*, "A silicon photonic biosensor using phase-shifted Bragg gratings in slot waveguide," *J. Biophoton.*, vol. 6, no. 10, pp. 821–828, Oct. 2013.

[23] Q. Fang *et al.*, "Carrier-induced silicon Bragg grating filters with a p-i-n junction," *IEEE Photon. Technol. Lett.*, vol. 25, no. 9, pp. 810–812, May 2013.

[24] M. Burla, L. Cortés, M. Li, X. Wang, L. Chrostowski, and J. Azaña, "Integrated waveguide Bragg gratings for microwave photonics signal processing," *Opt. Exp.*, vol. 21, no. 21, pp. 25120–25147, Oct. 2013.

[25] N. Berger, B. Levit, B. Fischer, M. Kulishov, D. V. Plant, and J. Azaña, "Temporal differentiation of optical signals using a phase-shifted fiber Bragg grating," *Opt. Exp.*, vol. 15, no. 2, pp. 371–381, Jan. 2007.

[26] W. Zhang and J. P. Yao, "A fully reconfigurable waveguide Bragg grating for programmable photonic signal processing," *Nature Commun.*, vol. 9, Apr. 2018, Art. no. 1396.

[27] W. Zhang and J. P. Yao, "Electrically programmable on-chip equivalent-phase-shifted waveguide Bragg grating on silicon," *J. Lightw. Technol.*, vol. 37, no. 2, pp. 314–322, Jan. 2019.

[28] K. O. Hill, B. Malo, F. Bilodeau, D. C. Johnson, and J. Albert, "Bragg gratings fabricated in monomode photosensitive optical-Fiber by UV exposure through a phase mask," *Appl. Phys. Lett.*, vol. 62, no. 10, pp. 1035–1037, Mar. 1993.

[29] T. Erdogan, "Fiber grating spectra," *J. Lightw. Technol.*, vol. 15, no. 8, pp. 1277–1294, Aug. 1997.

[30] C. R. Giles, "Lightwave applications of fiber Bragg gratings," *J. Lightw. Technol.*, vol. 15, no. 8, pp. 1391–1404, Aug. 1997.

[31] Y. J. Rao, "In-fibre Bragg grating sensors," *Meas. Sci. Technol.*, vol. 8, no. 4, pp. 355–375, Jan. 1997.
[32] R. A. Minasian, "Photonic signal processing of high-speed signals using fiber gratings," *Opt. Fiber Technol.*, vol. 6, no. 2, pp. 91–108, Apr. 2000.
[33] W. Zhang, W. Li, and J. P. Yao, "Optical differentiator based on an integrated sidewall phase-shifted Bragg grating," *IEEE Photon. Technol. Lett.*, vol. 26, no. 23, pp. 2383–2386, Dec. 2014.
[34] F. Li, Y. Park, and J. Azaña, "Complete temporal pulse characterization based on phase reconstruction using optical ultrafast differentiation (PROUD)," *Opt. Lett.*, vol. 32, no. 22, pp. 3364–3366, Nov. 2007.
[35] T. Yang *et al.*, "Experimental observation of optical differentiation and optical Hilbert transformation using a single SOI microdisk chip," *Sci Rep.*, vol. 4, Feb. 2015, Art. no. 3960.
[36] J. P. Yao, F. Zeng, and Q. Wang, "Photonic generation of ultrawideband signals," *J. Lightw. Technol.*, vol. 25, no. 11, pp. 3219–3235, Dec. 2007.
[37] Y. Park, M. Kulishov, R. Slavík, and J. Azaña, "Picosecond and subpicosecond flat-top pulse generation using uniform long-period fiber gratings," *Opt. Exp.*, vol. 14, no. 26, pp. 12670–12678, Dec. 2006.
[38] J. A. N. da Silva and M. L. R. de Campos, "Spectrally efficient UWB pulse shaping with application in orthogonal PSM," *IEEE Trans. Commun.*, vol. 55, no. 2, pp. 313–322, Feb. 2007.
[39] W. Zhang, N. Ehteshami, W. Liu, and J. P. Yao, "Silicon-based on-chip electrically tunable sidewall-Bragg-grating Fabry-Perot filter," *Opt. Lett.*, vol. 40, no. 13, pp. 3153–3156, Jul. 2015.
[40] W. Zhang and J. P. Yao, "Silicon-based on-chip electrically tunable phase-shifted waveguide Bragg grating for integrated microwave photonic applications," *in Proc. IEEE Int. Top. Meet. Microw. Photon.*, California, USA, Oct. 2016, pp. 309–312.
[41] W. Zhang and J. P. Yao, "Photonic generation of linearly chirped microwave waveforms using a silicon-based on-chip spectral shaper incorporating two linearly chirped waveguide Bragg gratings," *J. Lightw. Technol.*, vol. 33, no. 24, pp. 5047–5054, Dec. 2015.
[42] W. Zhang and J. P. Yao, "Silicon-based on-chip electrically-tunable spectral shaper for continuously tunable linearly chirped microwave waveform generation," *J. Lightw. Technol.*, vol. 34, no. 20, pp. 4664–4672, Oct. 2016.
[43] M. Jinno, H. Takara, B. Kozicki, Y. Tsukishima, Y. Sone, and S. Matsuoka, "Spectrum-efficient and scalable elastic optical path network: Architecture, benefits, and enabling technologies," *IEEE Commun. Mag.*, vol. 47, no. 11, pp. 66–73, Nov. 2009.
[44] O. Gerstel, M. Jinno, A. Lord, and S. J. B. Yoo, "Elastic optical networking: A new dawn for the optical layer?" *IEEE Commun. Mag.*, vol. 50, no. 2, pp. s12–s20, Feb. 2012.
[45] Y. Dai, X. Chen, D. Jiang, S. Xie, and C. Fan, "Equivalent phase shift in a fiber Bragg grating achieved by changing the sampling period," *IEEE Photon. Technol. Lett.*, vol. 16, no. 10, pp. 2284–2286, Oct. 2004.
[46] J. Li *et al.*, "Experimental demonstration of distributed feedback semiconductor lasers based on reconstruction-equivalent-chirp technology," *Opt. Exp.*, vol. 17, no. 7, pp. 5240–5245, 2009.
[47] W. Li, X. Zhang, and J. P. Yao, "Experimental demonstration of a multiwavelength distributed feedback semiconductor laser array with an equivalent chirped grating profile based on the equivalent chirp technology," *Opt. Exp.*, vol. 21, no. 17, pp. 19966–119971, Aug. 2013.
[48] J. Sun, C. W. Holzwarth, and H. I. Smith, "Phase-shift Bragg grating in silicon using equivalent phase-shift method," *IEEE Photon. Technol. Lett.*, vol. 24, no. 1, pp. 25–27, Jan. 2012.
[49] J. Sun *et al.*, "Uniformly spaced λ/4-shifted Bragg grating array with wafer-scale CMOS-compatible process," *Opt. Lett.*, vol. 38, no. 20, pp. 4002–4004, Oct. 2013.
[50] W. Zhang, W. Li, H. Shahoei, and J. P. Yao, "Independently tunable multichannel fractional-order temporal differentiator based on a silicon photonic symmetric Mach–Zehnder interferometer incorporating cascaded microring resonators," *J. Lightw. Technol.*, vol. 33, no. 2, pp. 361–367, Jan. 2015.
[51] R. Cheng and L. Chrostowski, "Multichannel photonic Hilbert transformers based on complex modulated integrated Bragg gratings," *Opt. Lett.*, vol. 43, no. 5, pp. 1031–1034, Mar. 2018.

Jianping Yao (M'99–SM'01–F'12) received the Ph.D. degree in electrical engineering from Universite de Toulon et du Var, Toulon, France, in December 1997. He is currently a Distinguished University Professor and University Research Chair with the School of Electrical Engineering and Computer Science, University of Ottawa, Ottawa, ON, Canada. From 1998 to 2001, he was with the School of Electrical and Electronic Engineering, Nanyang Technological University (NTU), Singapore, as an Assistant Professor. In December 2001, he joined the School of Electrical Engineering and Computer Science, University of Ottawa, as an Assistant Professor, where he was promoted to Associate Professor in May 2003, and to a Full Professor in May 2006. He was appointed as the University Research Chair in Microwave Photonics in 2007. In June 2016, he was conferred the title of Distinguished University Professor of the University of Ottawa. From July 2007 to June 2010 and July 2013 to June 2016, he served as the Director of the Ottawa-Carleton Institute for Electrical and Computer Engineering. He has authored or coauthored more than 620 research papers, including more than 360 papers in peer-reviewed journals and more than 260 papers in conference proceedings.

He is a registered Professional Engineer of Ontario. He is a Fellow of the Optical Society of America, the Canadian Academy of Engineering, and the Royal Society of Canada. He was an IEEE MTT-S Distinguished Microwave Lecturer for 2013–2015. He is Editor-in-Chief for the IEEE PHOTONICS TECHNOLOGY LETTERS, a Topical Editor for Optics Letters, an Associate Editor for Science Bulletin, a Steering Committee Member for JOURNAL OF LIGHTWAVE TECHNOLOGY, and an Advisory Editorial Board Member for Optics Communications. He was a Guest Editor of a Focus Issue on Microwave Photonics in Optics Express in 2013, a Lead Editor of a Feature Issue on Microwave Photonics in Photonics Research in 2014, and a Guest Editor of a Special Issue on Microwave Photonics in JOURNAL OF LIGHTWAVE TECHNOLOGY in 2018. He currently serves as the Chair of the IEEE Photonics Ottawa Chapter, and is the Technical Committee Chair of IEEE MTT-3 Microwave Photonics. He was a Member of the European Research Council Consolidator Grant Panel in 2016, the Qualitative Evaluation Panel in 2017, and a Member of the National Science Foundation Career Awards Panel in 2016. He has also served as a Chair of a number of international conferences, symposia, and workshops, including the Vice Technical Program Committee (TPC) Chair of the 2007 IEEE Topical Meeting on Microwave Photonics, TPC Co-Chair of the 2009 and 2010 Asia-Pacific Microwave Photonics Conference, TPC Chair of the high-speed and broadband wireless technologies subcommittee of the IEEE Radio Wireless Symposium 2009–2012, TPC Chair of the microwave photonics subcommittee of the IEEE Photonics Society Annual Meeting 2009, TPC Chair of the 2010 IEEE Topical Meeting on Microwave Photonics, General Co-Chair of the 2011 IEEE Topical Meeting on Microwave Photonics, TPC Co-Chair of the 2014 IEEE Topical Meetings on Microwave Photonics, and General Cochair of the 2015, and 2017 IEEE Topical Meeting on Microwave Photonics. He has also served as a Committee Member for a number of international conferences, such as IPC, OFC, BGPP, and MWP. He was the recipient of the 2005 International Creative Research Award of the University of Ottawa, the 2007 George S. Glinski Award for Excellence in Research, Natural Sciences and Engineering Research Council of Canada Discovery Accelerator Supplements Award in 2008, and the Award for Excellence in Research 2017–2018 of the University of Ottawa. He was selected to receive an inaugural OSA Outstanding Reviewer Award in 2012 and was one of the top ten reviewers of *Journal of Lightwave Technology* 2015–2016.

Weifeng Zhang (S'12–M'17) received the B.Eng. degree in electronic science and technology from Xi'an Jiaotong University, Xi'an, China, in 2008, the M.A.Sc. degree in electrical engineering from Politecnico di Torino, Torino, Italy, in 2011, and the Ph.D. degree in electrical engineering from the University of Ottawa, Ottawa, ON, Canada, in 2017. From June 2017 to May 2019, he was with the University of Ottawa, as a Postdoctoral Fellow. In June 2019, he joined the School of Information and Electronics, Beijing Institute of Technology, Beijing, China, as a Full Professor. His current research interests include silicon photonics and integrated microwave photonics.